Çukurova Üniversitesi
Mühendislik Fakültesi Dergisi
Çukurova University
Journal of the Faculty of Engineering
ISSN: 2757-9255 CİLT/VOLUME: 40 SAYI/ISSUE: 4 ARALIK/DECEMBER 2025

Current Status and Future Forecast of Global CO_2 Concentration Using Statistical and Deep Learning Time Series Methods

Sergen TUMSE [1,a]

[1]*Cukurova University, Engineering Faculty, Department of Mechanical Engineering, Adana,, Türkiye*

[a]***ORCID**: 0000-0003-4764-747X*

Article Info
Received : 02.09.2025
Accepted : 06.11.2025
DOI: 10.21605/cukurovaumfd.1776709

Corresponding Author
Sergen TUMSE
stumse@cu.edu.tr

Keywords
CO_2 concentration
Deep learning,
Global warming
Time series methods

***How to cite:** TÜMSE, S., (2025). Current Status and Future Forecast of Global CO_2 Concentration Using Statistical and Deep Learning Time Series Methods. Cukurova University, Journal of the Faculty of Engineering, 40(4), 875-888.*

ABSTRACT

In this study, four models were developed and assessed, including Autoregressive Integrated Moving Average (ARIMA), Feedforward Neural Network (FNN), Gated Recurrent Unit (GRU), and Long Short-Term Memory (LSTM) to evaluate current status and future forecast of global CO_2 concentration. A total of 554 global monthly datasets were employed to train and test the developed models, aimed at estimating future CO_2 concentrations. Then, each developed model was also utilized to estimate CO_2 concentrations for the future 110 months, from March 2025 to February 2035. Among all generated techniques, the LSTM model showed the highest estimation accuracy with an MAPE of 0.05%, an MAE of 0.2028 ppm, and an RMSE of 0.3216 ppm. Whereas GRU and FNN techniques also obtained good results with the same MAPE of 0.05%, their MAE and RMSE values were slightly higher. The four developed models (ARIMA, FNN, GRU, and LSTM) agree on a continuous rise in atmospheric CO_2 level within the range between March 2025 and early 2035, and they typically show CO_2 concentrations starting from approximately 425 ppm in early 2025 to 442-443 ppm by the end of 2034.

İstatistiksel ve Derin Öğrenme Zaman Serisi Yöntemleri Kullanılarak Küresel CO_2 Yoğunluğunun Mevcut Durumu ve Gelecekteki Tahmini

Makale Bilgileri
Geliş : 18.04.2025
Kabul : 27.05.2025
DOI: 10.21605/cukurovaumfd.1776709

Sorumlu Yazar
Sergen TUMSE
stumse@cu.edu.tr

Anahtar Kelimeler
Karbondioksit emisyonu
Derin öğrenme
Küresel ısınma
Zaman serisi yöntemleri

***Atıf şekli:** TÜMSE, S., (2025). İstatistiksel ve Derin Öğrenme Zaman Serisi Yöntemleri Kullanılarak Küresel CO_2 Yoğunluğunun Mevcut Durumu ve Gelecekteki Tahmini. Çukurova Üniversitesi, Mühendislik Fakültesi Dergisi, 40(4), 875-888.*

ÖZ

Bu çalışmada global CO_2 yoğunluğunun güncel durumunu ve gelecek tahminini değerlendirebilmek amacıyla, Otoregresif Entegre Hareketli Ortalama (ARIMA), İleri Beslemeli Sinir Ağı (FNN), Kapılı Yinelemeli Birim (GRU) ve Uzun Kısa Süreli Bellek (LSTM) olmak üzere dört model geliştirilmiştir. Gelecekteki CO_2 yoğunluklarını tahmin etmeyi amaçlayan bu modelleri eğitmek ve test etmek için toplam 554 aylık veri kullanılmıştır. Daha sonra geliştirilen her model, Mart 2025'ten Şubat 2035'e kadar olan 110 aylık süre için CO_2 yoğunluklarını tahmin etmek için de kullanılmıştır. Oluşturulan tüm teknikler arasında LSTM modeli, %0,05'lik bir MAPE, 0,2028 ppm'lik bir MAE ve 0,3216 ppm'lik bir RMSE ile en iyi tahmin doğruluğunu göstermiştir. GRU ve FNN teknikleri de aynı %0,05'lik MAPE ile iyi sonuçlar elde ederken, MAE ve RMSE değerleri biraz daha yüksek çıkmıştır. Geliştirilen dört model (ARIMA, FNN, GRU ve LSTM), Mart 2025 ile 2035 başı aralığında atmosferik CO_2 seviyesinde sürekli bir artış ve tipik olarak CO_2 yoğunluğunun 2025 başı yaklaşık 425 ppm'den başlayarak 2034 sonu itibarıyla 442-443 ppm arasına çıkması konusunda hemfikirdir.

1. INTRODUCTION

The significant impacts of global climate change and its outcomes have made it exceptionally important to accurately measure carbon emissions. The release of greenhouse gases plays a key role in driving global warming and exacerbating the environmental challenges related to climate change. Some regions of the world, having a greater impact on carbon emissions, lead to significant environmental and health issues. The magnitude of these problems requires creative solutions for the future of the world and humanity. Human activities such as burning fossil fuels, destroying forests, and using some traditional farming methods release large quantities of greenhouse gases, mainly carbon dioxide (CO_2) to the atmosphere. The global quantity of CO_2 produced in 2022 exceeded 2021 levels by nearly 1.5% [1]. After two sequential years characterized by unusual fluctuations in energy-related carbon emissions, an increase was detected last year. The COVID-19 pandemic rapidly reduced energy consumption in 2020, resulting in a decrease in emissions of more than 5%. Global CO_2 emissions rose by over 6%, exceeding pre-pandemic quantity, as economic recovery was driven by financial support and the widespread administration of vaccinations in 2021 [2]. Climate change creates an extraordinary environmental and societal challenge, with results that threaten the health, safety, and livelihoods of billions of people globally [3,4].CO_2 emissions contribute to climate change. Analyzing CO_2 emissions is of great importance for combating climate change. Machine learning programs are becoming increasingly important for systematically monitoring CO_2 emissions.

Artificial intelligence has a major role in every field this century, facilitating many areas. Artificial intelligence, especially through the use of ML techniques, has gained significant importance for environmental sustainability. Machine learning methods are progressively accepted for supporting decision-making for environmental sustainability, especially in forecasting current CO_2 levels and estimating future emission levels [5].

Machine learning includes a diverse set of computational methodologies that deduce patterns from data, enabling the analysis of wide-reaching datasets and the modeling of nonlinear dynamics. Autoregressive Integrated Moving Average (ARIMA) models and Long Short-Term Memory (LSTM) networks are two widely adopted methodological frameworks for forecasting CO_2 emissions [6,7]. In the study of Nuaimi et al. [8], various machine learning algorithms such as Artificial Neural Networks, Support Vector Machines, Extreme Learning Machines, and Ensemble Methods have been used to predict carbon emissions. This study emphasizes the strengths and limitations of the proposed models. According to authors, the automation of hyperparameter optimization and model training can remarkably improve the performance of emissions prediction techniques. Ma et al. [9] developed different algorithms to predict the CO_2 emission by utilizing 21 operating parameters from a municipal solid waste (MSW) incineration plant as input parameters. The outcomes demonstrated a powerful estimation performance for the generated algorithms, Random Forest (RF) and XGBoost, with coefficient of determination, R^2=0.932 and 0.903, respectively. Begum and Mobin [10] applied six machine learning techniques to forecast CO_2 emissions through 2030 for the eleven maximum-emitting countries. They determined the mean estimation accuracy to be 96.21%. According to them, Russia is projected to exceed its specified decreasing commitments, in contrast to Germany and the United States, which are expected to experience small shortfalls in reaching their respective objectives. Alhussan et al. [11] proposed a detailed framework that combines advanced deep learning models containing Gated Recurrent Unit (GRU), Bidirectional GRU (BiGRU), Stacked GRU, and Attention-enhanced BiGRU with a unique hybrid optimization model, GGBERO, advanced by the combination of Greylag Goose Optimization (GGO) and the Al-Biruni Earth Radius (BER) technique. According to them, besides improving the estimation accuracy of CO_2 emissions, the introduced combined framework supplies remarkable insights into the main determinants of CO_2 emissions, thus helping policymakers and researchers, in making informed, data-driven decisions for diminishing climate change effects. Ayaz [12] compared the conventional ARIMA model and deep learning based LSTM model to assess current and future levels of CO_2 emissions in Türkiye, utilizing the data from the Global Carbon Atlas published in 2023. According to the results, the LSTM algorithm yielded the coefficient of determination as R^2 = 90.4%, whereas the ARIMA algorithm yielded an R^2 score of 94.3%. The author stated that machine learning models are critical tools in mitigating climate change effects and provide

valuable insights to policymakers. Uluocak [13] investigated the estimations of CO, CO_2 and NO_x emissions from a diesel engine using two deep learning time series methods such as GRU and LSTM neural networks. According to results, the developed LSTM model demonstrated better accuracy in estimating CO_2 emissions whereas the GRU model yielded superior performance in estimating CO and NO_x emissions. Korkmaz [14] developed linear regression, XGBoost and kNN models to predict CO_2 emissions of vehicles. The results revealed that XGBoost model yields best accurate CO_2 emission values with a RMSE of 6.45, a MAE of 2.81 and R^2 of 0.9875.

The aim of this study is to predict the current and future trend of CO_2 by using 554 global monthly mean CO_2 concentration data recorded between January 1979 and February 2025 at the Mauna Loa Observatory, operated by the National Oceanic and Atmospheric Administration (NOAA) using four different models: Autoregressive Integrated Moving Average (ARIMA), Feedforward Neural Network (FNN), Gated Recurrent Unit (GRU), and Long Short-Term Memory (LSTM).

2. METHODS

2.1. Data Description

The data employed in this investigation include global monthly average CO_2 concentrations (ppm) recorded by the National Oceanic and Atmospheric Administration (NOAA)'s Mauna Loa Observatory for dates between January 1979 and February 2025. Before model applications, detailed preprocessing steps were established to improve the effectiveness and utility of the dataset for time series prediction. First, the raw atmospheric CO_2 concentration data were normalized utilizing the min-max scaling method. This technique converted the data into a uniform range between 0 and 1, thus providing stable and effective neural network training by diminishing the impact of differing magnitudes. The dataset including 554 global monthly records between January 1979 and February 2025 was separated into training and testing subsets in such a way, 80% of the dataset was used for model training that the remaining 20% was allocated for the testing process. To provide sequential modeling, the normalized data were arranged in input-output pairs in which each input sequence included a constant number of past months' data, which was utilized to estimate CO_2 concentration values of the following months. This arrangement allowed the models to handle both short-term fluctuations and long-term dependencies in the atmospheric CO_2 concentration time series distribution.

2.2. Autoregressive Integrated Moving Average (ARIMA)

ARIMA models are used when the output variable is affected not only by the current data but also by previous information. These models can only be employed for fixed time series data, so the data must first be checked and transformed, if required, to guarantee stationarity before model application. It is primarily applied for two purposes: to examine time series data for deeper insights and to estimate future trends. As an autoregressive statistical approach, ARIMA predicts further data using previous observations. A prevalent implementation of ARIMA models is the estimation of stock market prices, where forward prices of a stock are predicted utilizing its historical data. An ARIMA model is constituted of three components: AR, I, and MA. The "AR" means to autoregression, referring the variable is expressed by its own past values. This kind of model predicts future values from preceding records. The "I" refers "integrated," meaning to the differencing of time series data to provide stationarity. If a dataset is not fixed, it can be made stationary by modifying each data point by the difference between this value and its previous value. The final constituent, "MA," refers Moving Average and demonstrate the model's error as a linear combination of previous estimation errors [15]. ARIMA models can only be applied on stationary time series; in other words, non-stationary data must be converted before model building. Thus, the first step in creating an ARIMA model is to be sure the data are stationary [16]. Figure 1 demonstrates the structure of the ARIMA model.

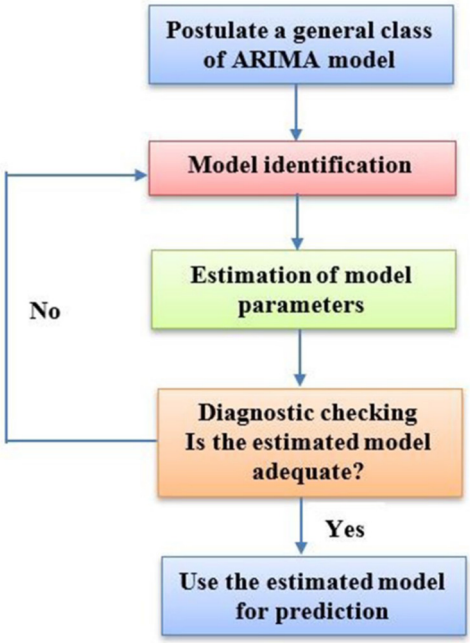

Figure 1. The structure of the ARIMA model [17]

2.2.1. Moving Average (MA) Process

A sequence $\{z_t\}$ is described as a moving average process of order q when it provides the defining circumstances.

$$z_t = a_t - \theta_1 a_{t-1} - \theta_2 a_{t-2} - \ldots - \theta_q a_{t-q} \quad (1)$$

In Equaiton (1), θ_i; i=1,2,3…q are fixed constants whereas $\{a_t\}$shows simply random process with zero mean and variance σ^2 [11].

2.2.2. Autoregressive (AR) Process

A sequence $\{z_t\}$ is described as an autoregressive process of order q when it fulfills the defining characteristics.

$$z_t = \phi_1 z_{t-1} - \phi_2 z_{t-2} - \ldots - \phi_p z_{t-p} + a_t \quad (2)$$

In Equation (2), ϕ_i; i=1,2,3…p are fixed constants whereas $\{a_t\}$shows simply random process with zero mean and variance σ^2 [11].

This model runs in a similar manner to multiple regression models.

2.2.3. Autoregressive Moving Average (ARMA) Process

The autoregressive (AR) and moving average (MA) constituents are associated with each other to create the autoregressive moving average (ARMA) model. For a time series, the ARMA(p,q) model, which contains p (AR) components and q (MA) components, can be demonstrated as follows.

$$z_t = \sum_{i=1}^{p} \phi_i x_{t-i} - \sum_{i=1}^{q} \theta_j a_{t-j} + a_t \; ; t = 1, \ldots, T \quad (3)$$

In Equation (3), a_t describes a classic white noise process including zero mean and variance σ^2. Here, the sign T denotes the time series length [18]. For validity, the AR components must satisfy the stationarity condition, whereas the MA components are needed to provide the invertibility condition.

2.3. Feed-forward Neural Network

Neural networks (NN) are improved computational techniques inspired by the constitution and mechanism of the human central nervous system [19]. Essentially, an NN applies nonlinear mapping, converting an available input value into a corresponding output pattern. A simple NN is constituted of connected artificial neurons or nodes, adjusted through three main layers, namely the input, hidden, and output layers. A neural network (NN) including a sufficient number of hidden nodes can predict any nonlinear function. But, the neuron number in the hidden layer depends on the type of problem involved, and they should be optimized to hinder overfitting [20]. Even though NNs have the capability of mapping an input value to the output pattern, they must be trained to understand the patterns of distribution in datasets to achieve successful mappings. The main aim of the training process is to specify the optimum set of biases and weights that reduce the error possibility of the developed network [21]. The training process can be carried out across supervised, unsupervised, or reinforcement learning. Determining a suitable training algorithm is a crucial issue of applying NNs [22]. Equation (4) explains the operation of neural networks in the estimation of a parameter. According to Equation (4), while the predicted value is specified as F and the output bias value is denoted by the symbol a, w_{ij} and v_j are called weights of input and output layers, respectively. Furthermore, the number of nodes in the hidden layer is represented by h; the number of input parameters is denoted by k, whereas x is used to describe the input variable.

$$F = f\left(a + \sum_{j=1}^{h} v_j + \sum_{i=1}^{k} g w_{ij} x_i + b_j \right) \tag{4}$$

A feed-forward neural network (FNN) is the oldest and simplest type of artificial neural networks. In this technique, knowledge or data flows in only one direction, such as from the input layer to the output layer, and it does not include any feedback and recurrent interconnections [23]. A multilayer FNN is composed of multiple neuron layers connected sequentially in the forward direction [24].

2.4. Long Short-Term Memory (LSTM)

Hochreiter [25] played a key role in the progress of the LSTM model. Even though initially considered a kind of recurrent neural network (RNN), this technique solves the restrictions of classic RNNs by offering memory cells, or cell states, which help to diminish the gradient problem. The architecture of an LSTM layer is demonstrated in Figure 2. This figure demonstrates how a time series X, described by C properties (channels) and length S, is operated through the LSTM layer. Additionally, the hidden state specified as ht serves as both an output and an explanation of the cell's condition at time step t. The LSTM unit produces the first output while synchronously updating the cell state at the first time step and for the initial network state. When the sequence proceeds, the LSTM component applies the preceding cell and hidden states (c_{t-1}, h_{t-1}) to simultaneously calculate the updated cell state (c_t) and the output at time step t [26].

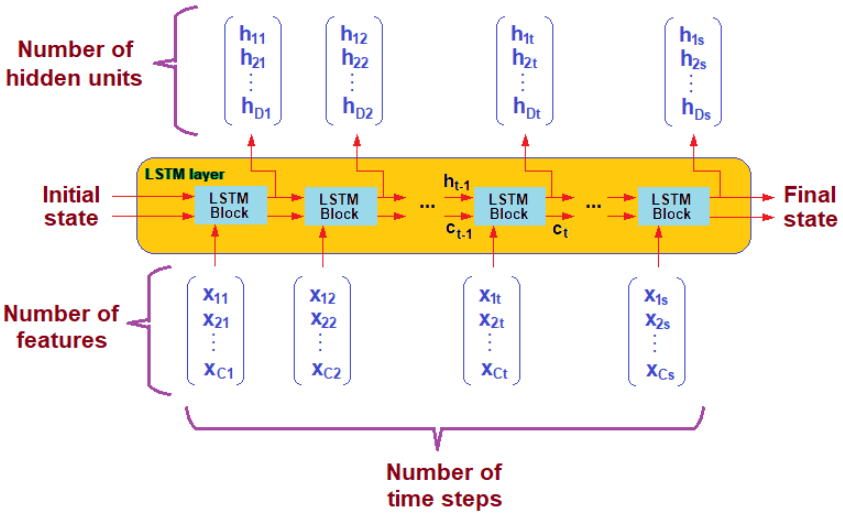

Figure 2. Schematic demonstration of an LSTM layer [26]

The LSTM model has three kinds of learnable components, namely input weights (W), recurrent weights (R), and biases (b). Furthermore, three matrices are constructed to contain these components for each gate. The united structure of these three matrices for all gate constituents is illustrated in Equation (5).

$$W = \begin{bmatrix} W_i \\ W_f \\ W_g \\ W_o \end{bmatrix}, R = \begin{bmatrix} R_i \\ R_f \\ R_g \\ R_o \end{bmatrix}, b = \begin{bmatrix} b_i \\ b_f \\ b_g \\ b_o \end{bmatrix} \quad (5)$$

In Equation (5), while the input gate is described with *i*, the forget gate and cell candidate are denoted with *f* and *g*, respectively. On the other hand, the sign '*o*' represents the output gate, as demonstrated in each weight matrix.

2.5. Gated Recurrent Unit (GRU)

Gated recurrent unit (GRU) is a kind of recurrent neural network (RNN) with a simplified structure compared to LSTM to improve computational performance and accuracy. The internal component of the GRU is analogous to that of LSTM, except that it combines LSTM's forget and input gates into a single update port. This technique is inspired by the LSTM model but is considered easier to comment on and apply. This property enables the LSTM to solve the vanishing gradient issue. The internal structure of GRU is simpler, which facilitates a simpler training process compared to other models since it demands low computational effort to enhance its parameters. The reset gate identifies whether data or knowledge from the preceding state should be unified with data or knowledge of the current state. The update gate checks the extent to which data or knowledge from the preceding state is maintained in the present state. Figure 3 illustrates the GRU model structure. The subsequent equations explain the mathematical procedures that govern the GRU cell gating system [27]:

$$z_t = \sigma(x_t W^z + h_{t-1} U^z + b_z) \quad (6)$$

$$r_t = \sigma(x_t W^r + h_{t-1} U^r + b_r) \quad (7)$$

$$\tilde{h}_t = \tanh[(r_t \times h_{t-1} U + x_t W + b)] \quad (8)$$

$$h_t = (1 - z_t) \times \tilde{h}_t + z_t \times h_{t-1} \quad (9)$$

In these equations, the weight matrices related to the present input vector are defined as W^z, W^r, and W. On the other hand, the weight matrices of previous time steps are denoted as U^z, U^r, and U. Bias parameters are described with the symbols b_z, b_r, and b. Moreover, while the sign σ defines logistic sigmoid function, z_t present updating gate, r_t is reset gate and $\tilde{h}_t$ describes the candidate's secret layer [28].

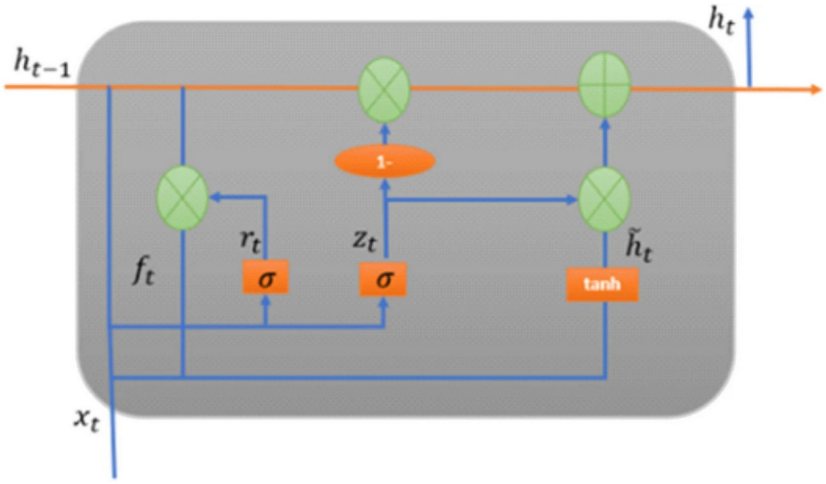

Figure 3. The schematic illustration of the GRU model structure [27]

In the current investigation, LSTM and GRU models were implemented to predict present and future CO_2 concentrations. The developed architectures were assessed by changing the number of hidden units between 5 and 100 with an interval of 5. Training was performed for 500 epochs. The learning rate, which is a main parameter for model convergence, was examined for values between 0.005 and 0.5. With respect to performance evaluations, the most accurate LSTM model was achieved by including 75 hidden units. The Adam optimizer was utilized for the update of parameters, whereas the hyperbolic tangent (tanh) was used for the activation function. The dimensions of the input layer were adjusted to one for the developed LSTM and GRU architectures.

3. RESULTS AND DISCUSSIONS

3.1. Model Evaluation and Historical Forecasts (2016-2025)

As can be seen in Figure 4, during the testing phase, a comprehensive comparison is conducted for the period from 2016 to 2025 between actual atmospheric CO_2 concentrations (in ppm) and their corresponding predicted values generated by an ARIMA (Autoregressive Integrated Moving Average) model. In order to prevent any misunderstanding, the actual CO_2 values are represented as a continuous blue line, whereas the ARIMA forecasted values are depicted as a red dashed line. Figure 4 presents the robustness of the ARIMA model to monitor both the long-term upward trend in atmospheric CO_2 content and the short-term seasonal oscillations. For example, at the beginning of 2016, the actual CO_2 level in the atmosphere was measured at 402.64 ppm, and the value reached 426.05 ppm by 2025. Likewise, by employing the ARIMA model, the forecasted CO_2 level in the atmosphere is estimated to be 401.12 ppm, in the beginning of 2016, while this value is projected to reach 424.31 ppm, in the beginning of 2025. According to these results, while the real CO_2 concentration rise is recorded as 23.41 ppm, this value is observed as 23.19 ppm with the ARIMA model between 2016 and 2025. Moreover, these perfect matchings also hold for the rest of the values, as can be seen in Figure 4, which proves the model's strong ability to capture the trend.

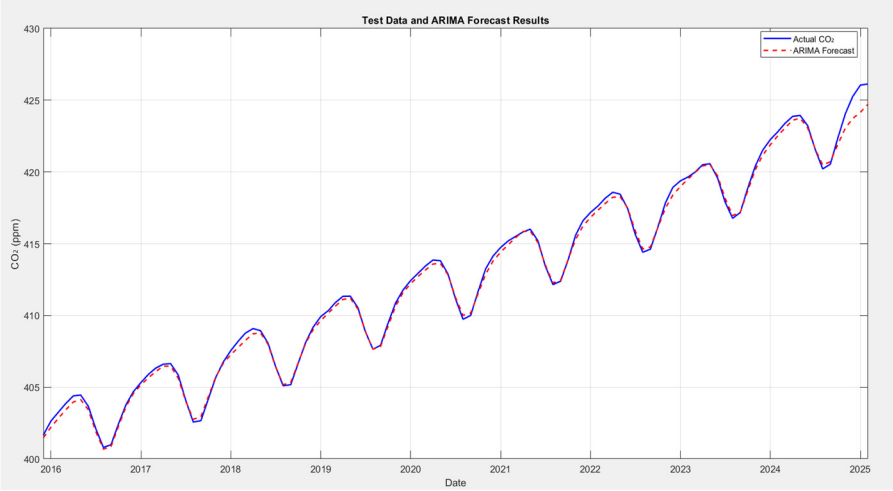

Figure 4. Comparison of actual and predicted CO_2 concentrations with ARIMA model in testing stage

Aside from the ARIMA model, another powerful model, the Feedforward Neural Network (FNN), is applied and illustrated in Figure 5. The figure represents a clear comparison between recorded CO_2 concentrations and the FNN model's predictions during the testing phase. To avoid any misinterpretation, the actual CO_2 values are denoted as a blue line, and the FNN forecasts are plotted as a red dashed line. These lines demonstrate nearly perfect correlations, which indicate the model's ability to monitor both the increasing tendency of CO_2 levels and the regional fluctuations of atmospheric CO_2 concentrations. For instance, in May 2016, the actual CO_2 content was recorded as approximately 404.45 ppm, while the suggested FNN model predicted 404.23 ppm. As can be seen in Figure 5, true values of CO_2 and the simulated values agree well with each other. Slight deviations exist between collected CO_2 and estimated CO_2 data, ranging from October 2024 to early 2025. The corresponding values are 422.87 ppm for actual CO_2 and 422.51 ppm for forecasted CO_2 model in October 2024, with values in early 2025 being 426.08 ppm for true CO_2 level and 424.78 ppm for predicted CO_2 content in the atmosphere. Although small

differences are noticeable in certain local regions, those disagreements are minimal and do not affect the overall performance of the proposed model. Furthermore, this situation contributes to the model's sensitivity to the natural variability, and highlights the model's capability of replicating the seasonal changes in atmospheric CO_2 levels.

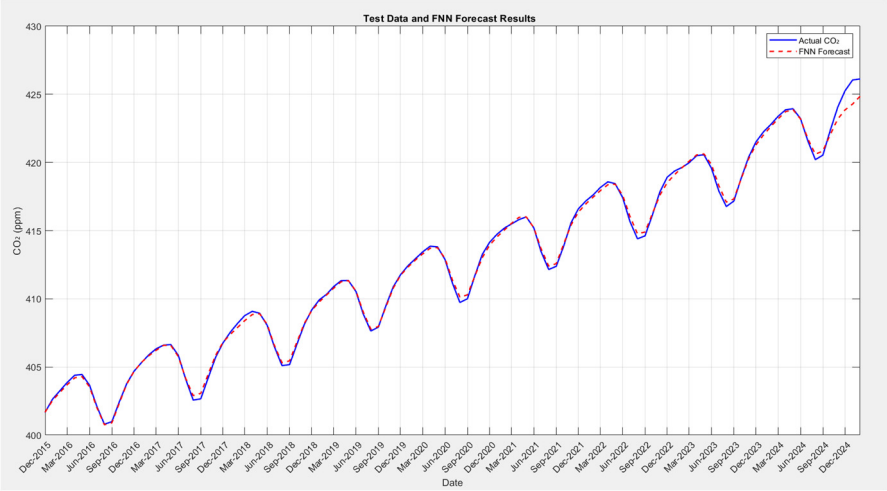

Figure 5. Comparison of actual and predicted CO_2 concentrations with FNN model in testing stage

To provide better performance analysis, the Gated Recurrent Unit (GRU) model is employed to forecast the atmospheric CO_2 concentrations. Here, Figure 6 visualizes the GRU model's prediction capacity during the implementation phase, which covers the period from late 2015 to early 2025. To provide a clear image, the actual CO_2 data are represented as a continuous blue line, while the GRU data are presented as a red dashed line. As can be inferred, the GRU model accomplishes the annual increase and seasonal fluctuations, and achieves strong alignment with the observed long-term growth pattern. For example, in the year 2020, the real CO_2 level is measured as 412.42 ppm, while the forecasted CO_2 value is estimated as 412.34 ppm. Furthermore, these perfect matchings are also applicable to the data presented in Figure 6. A few small differences are observed at the end of 2024. An example of the major deviation the true value of CO_2 at the beginning of 2025 is measured as 426.10 ppm, whereas the projected CO_2 content is 424.39 ppm. Thus, the differences are in the acceptable range, and to further validate the robustness of the proposed model, a quantitative evaluation table (Table 1) is generated. From Table 1, the Root Mean Square Error (RMSE) value is calculated as 0.3342 ppm, which indicates low standard deviation, and demonstrates the soundness of the model.

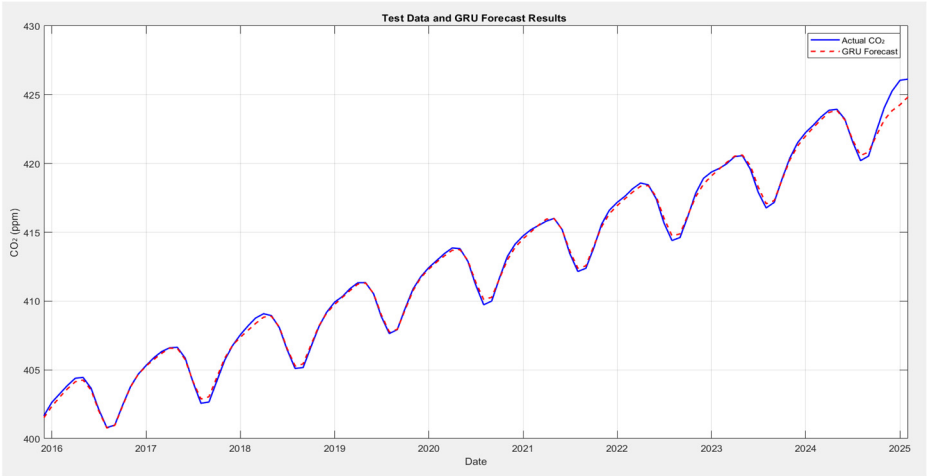

Figure 6. Comparison of actual and predicted CO_2 concentrations with GRU model in testing stage

Finally, an alternative machine learning model, the Long Short-Term Memory (LSTM), was performed, and its predictive performance is plotted in Figure 7 during the testing period ranging from late 2015 to 2025. The true CO_2 values are demonstrated as a continuous blue line, while the forecasted LSTM data is

denoted as a red dashed line. Likewise, the LSTM effectively captures the increasing trend, and the model shows good agreement with the measured CO_2 concentrations. As an example of this, the peak values of the forecasted and actual CO_2 levels in 2023 are found to be exactly 420.48 ppm for both. This perfect correlation is valid in most cases throughout the time series. While minor deviations occur at certain turning points of the seasonal curve, these differences are minimal and remain in the acceptable range. For example, an obvious deviation occurs at the end of 2024, and the corresponding values are 424.07 ppm for the proposed model, but it is 426.05 ppm for the recorded CO_2 concentrations. As can be seen, the percentage differences are calculated as less than 1%. the quantitative results tabulated in Table 1 further validate the model's ability to reflect the data.

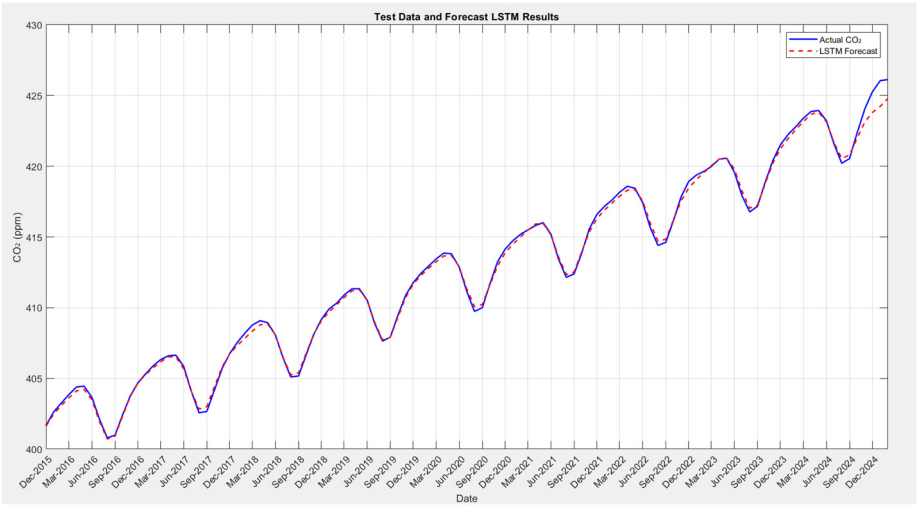

Figure 7. Comparison of actual and predicted CO_2 concentrations with LSTM model in testing stage

According to Table 1, among all generated techniques, the LSTM model showed the best estimation accuracy with a MAPE of 0.05%, a MAE of 0.2028 ppm, and an RMSE of 0.3216 ppm. Whereas GRU and FNN techniques also obtained good results with the same MAPE of 0.05%, their MAE and RMSE values were a bit greater. On the other hand, the conventional statistical approach, which is called as ARIMA model, yielded the worst performance with a MAPE of 0.06%, a MAE of 0.2488 ppm, and an RMSE of 0.3672 ppm, revealing limited ability in handling nonlinear trends and seasonal dynamics. The results in Table 1 reveal the strong performance of deep learning models—particularly LSTM—in modeling complex environmental time series such as atmospheric CO_2. The LSTM's internal memory mechanism allows it to effectively capture long-term dependencies and seasonal variations in the data.

Table 1. Error metrics for the developed models

Model	MAPE (%)	MAE (ppm)	RMSE (ppm)
ARIMA	0.06	0.2488	0.3672
FNN	0.05	0.2036	0.3246
GRU	0.05	0.2145	0.3342
LSTM	0.05	0.2028	0.3216

3.2. Future Predictions (2025-2035)

In Figure 4, ARIMA-based and actual CO_2 concentrations are presented and compared extensively during the testing stage from 2016 to 2025. The near-perfect matching observed between real CO_2 and predicted values which proves the validity and precision of the model. Accordingly, in Figure 8, the extended version of the ARIMA model, is forecasted from March 2025 to December 2035. The model exhibits a continued increase in atmospheric CO_2 concentration, starting from approximately 426 ppm to around 444 ppm by the end of 2035. The model also clearly reveals the different seasonal oscillations, which indicate its capability of monitoring cyclical and distinct trend components through the decades. Furthermore, the average predicted CO_2 concentration in 2025 is found to be 424.98 ppm, while the 2026 estimate is 426.84 ppm, and the increase is calculated as 1.86 ppm. According to the ARIMA model, the average annual raise is calculated as around 1.8 ppm per year up to 2035, which is consistent with historical growth rate, and the

total increase from 2025 to 2035 is detected as 18.38 ppm. This compactness validates the model's future monitoring capabilities and demonstrates its ability to maintain accurate and dependable long-term estimations.

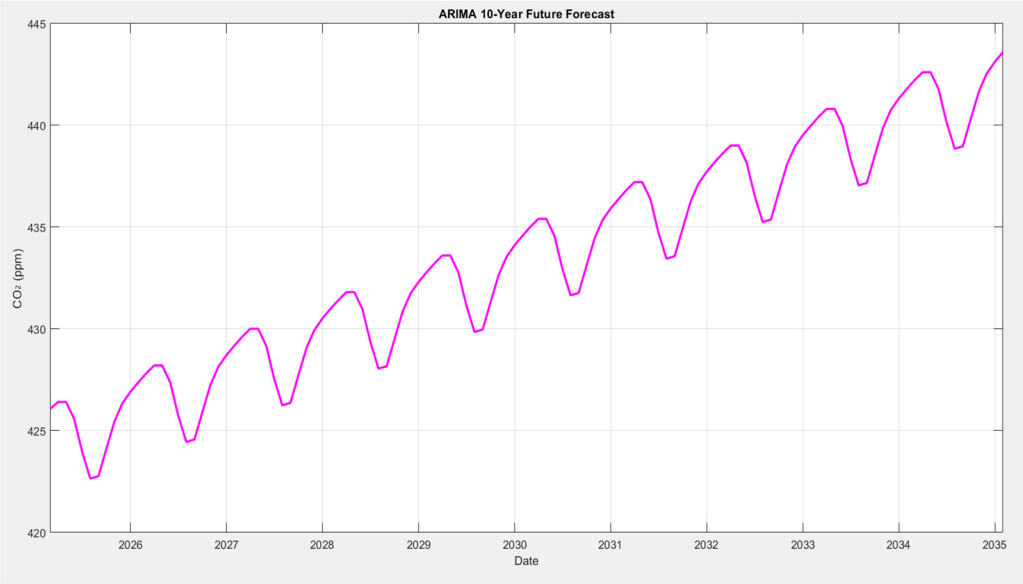

Figure 8. Predicted CO_2 concentration in future from March 2025 to December 2033 with ARIMA model

The testing performance of the Feedforward Neural Network (FNN) from late 2016 to the end of 2024 was represented in Figure 5, and a wide-ranging comparison was made between observed and predicted CO_2 concentrations. According to Figure 5, the real and forecasted CO_2 data are in good agreement and the FNN model can accurately determine both the trend and the seasonal changes. The long-term FNN estimations for the period 2025-2035 are demonstrated in Figure 9. Similar to the ARIMA model, the FNN model predicts a continuous increase in CO_2 level in the atmosphere, reaching up to 442.65 ppm by early 2035. For example, the average projected CO_2 concentration for 2025 is determined as 424.18 ppm, while the arithmetical mean of CO_2 content for 2026 is depicted as 425.99 ppm, and the difference between these two years are calculated as 1.81 ppm, which is 0.05 ppm less than the ARIMA model. Throughout the forecasting data, CO_2 levels in the atmosphere rise around 4% from 425.21 ppm on the first of March 2025 to 442.65 ppm on the first of February 2035. Those findings state that the suggested FNN model clearly simulates the future of atmospheric CO_2 levels, confirming the expected increase in CO_2 contents while precisely capturing the seasonal variability.

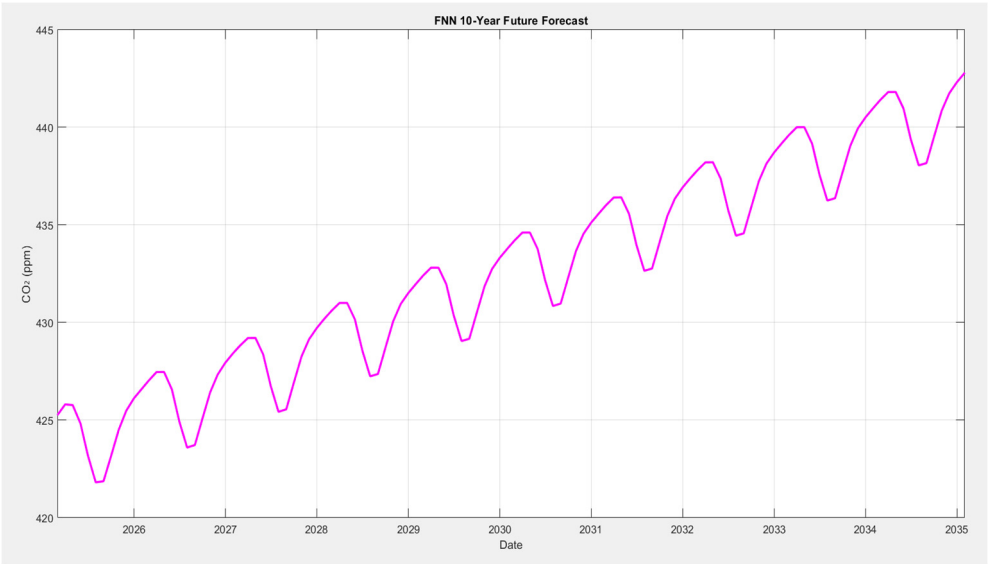

Figure 9. Predicted CO_2 concentration in future from March 2025 to December 2033 with FNN model

In Figure 6, the performance of the Gated Recurrent Unit (GRU) model is specified for atmospheric CO_2 concentration predictions from 2016-2025, during the testing phase. Additionally, the trained GRU model is briefly implemented on the unseen data to evaluate its forecasting accuracy against actual observations. In Figure 10, based on the GRU model's validated performance, the GRU is employed to generate a long-term CO_2 level forecast from March 2025 to December 2035. According to Figure 10, the atmospheric CO_2 value increases from 425.20 ppm in early 2025 to 442.84 ppm by the end of 2035. Similar to Figure 6, the proposed model successfully simulates the characteristics of seasonal oscillations across the forecasted years, which validates the model's capacity to extend sequential dependencies into the future for monitoring. For instance, the peak of CO_2 level is estimated to be 427.46 ppm in May 2026, while the highest CO_2 concentration is found to be 429.26 ppm in May 2027. For the selected years, the GRU model's forecast differences between May 2026 and May 2027 are found to be 1.8 ppm, whereas the FNN model's findings for the same time period are found to be 1.7 ppm, which is 0.1 ppm less than the GRU model's outputs. Both models predict an increase in CO_2 value and suggest almost identical values, which demonstrates the models' excellent predictive capability.

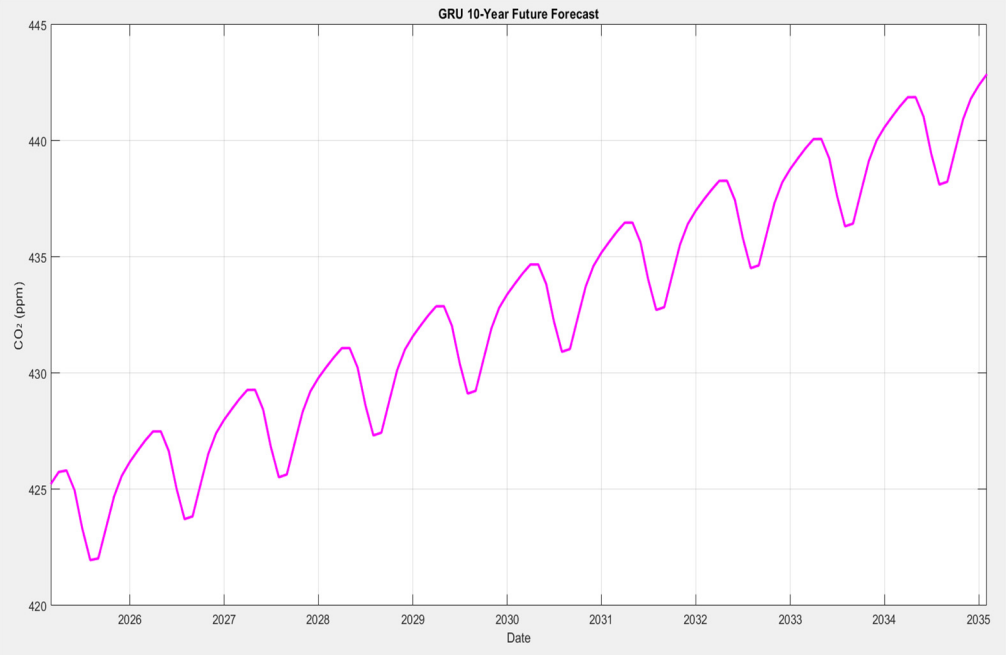

Figure 10. Predicted CO_2 concentration in future from March 2025 to December 2033 with GRU model

A testing capacity of the Long Short-Term Memory (LSTM) model is demonstrated in Figure 7 for the atmospheric CO_2 prediction from 2016 to 2025. Figure 7 briefly explores the robustness of the trained LSTM network, which is trained on invisible data to estimate the forecasting accuracy against the true observations. Furthermore, the performance metrics reported in Table 1 demonstrate the robustness of the LSTM algorithm. In Figure 11, a wide range of future atmospheric CO_2 concentration analyses is considered, starting from March 2025 to December 2034. Likewise, those findings suggest a steady increase in CO_2 availability in the atmosphere from 425.23 ppm to 442.26 ppm across the time interval. More specifically, the lowest CO_2 level is determined to be 435.71 ppm in August 2033 and the lowest CO_2 value is 437.51 ppm in August 2034; the total increase is detected to be 1.8 ppm. Also, quite similar increases in CO_2 content are observed in other models, which generalizes the learned sequential dependencies beyond the training period. All in all, the four models (ARIMA, FNN, GRU, and LSTM) agree on a continuous rise in atmospheric CO_2 levels between March 2025 and early 2035, with CO_2 concentrations starting from approximately 425 ppm in early 2025 to between 442 - 443 ppm by the end of 2034. Despite methodological variations, each model independently confirms a steady increase in atmospheric CO_2 values of 1.7-1.9 ppm per year. This multi-model agreement highlights the reliability of the model's future projections and the soundness of the forecasting framework.

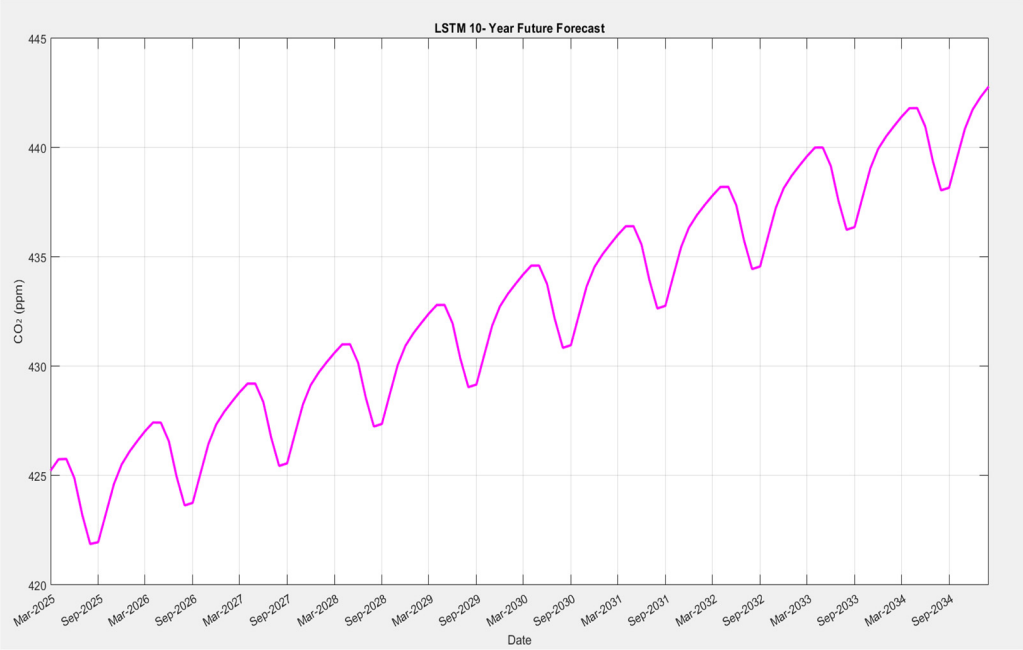

Figure 11. Predicted CO_2 concentration in future from March 2025 to December 2033 with LSTM model

4. CONCLUSIONS

In this study, various models were developed to estimate current and future CO_2 concentrations by using data recorded between January 1979 and February 2025. Four different models were generated and compared with each other, namely ARIMA, FNN, GRU, and LSTM. A total of 554 global monthly data points were applied to train and test generated models. Then each developed model was also used to forecast CO_2 concentrations for the future 110 months, from March 2025 to February 2035. Among all developed models, the LSTM model yielded the best prediction accuracy with a MAPE of 0.05%, an MAE of 0.2028 ppm, and an RMSE of 0.3216 ppm. Whereas GRU and FNN techniques also obtained good results with the same MAPE of 0.05%, their MAE and RMSE values were a bit greater. On the other hand, the conventional statistical approach, which is called the ARIMA model, yielded the worst performance with an MAPE of 0.06%, an MAE of 0.2488 ppm, and an RMSE of 0.3672 ppm, revealing limited ability in handling nonlinear trends and seasonal dynamics. The four models (ARIMA, FNN, GRU, and LSTM) agree on a continuous rise in atmospheric CO_2 level between March 2025 and early 2035, predicting CO_2 concentrations starting from approximately 425 ppm in early 2025 to between 442 to 443 ppm by the end of 2034. Despite methodological variations, each model independently confirms a steady increase in atmospheric CO_2 values at an average increase of 1.7-1.9 ppm per year. This multi-model agreement highlights the model's reliability of the future projections and the sound of the forecasting framework. The results of this work reveal the strong performance of the LSTM technique in modeling complex environmental time series such as atmospheric CO_2. This study shows the applicability and accuracy of AI-based prediction techniques in climate-related applications and supplies a stable methodological framework for future investigation in environmental monitoring, climate policy planning, and data-driven sustainability initiatives.

5. REFERENCES

1. Liu, Z., Deng, Z., Davis, S. & Ciais, P. (2023). Monitoring Global Carbon Emissions in 2022. *Nature Reviews Earth & Environment, 4*(4), 205-206.
2. Liu, B., Chang, H., Li, Y. & Zhao, Y. (2023). Carbon emissions predicting and decoupling analysis based on the PSO-Elm combined prediction model: Evidence from chongqing municipality, China. *Environmental Science and Pollution Research, 30*(32), 78849-78864.
3. Wang, B. & Liu, J. (2024). Impact of climate change on green technology innovation-an examination based on microfirm data. *Sustainability, 16*(24), 11206.

4. Arora, N.K. (2019). Impact of climate change on agriculture production and its Sustainable Solutions. *Environmental Sustainability, 2*(2), 95-96.

5. Fan, Z., Yan, Z. & Wen, S. (2023). Deep Learning and Artificial Intelligence in sustainability: A review of sdgs, renewable energy, and environmental health. *Sustainability, 15*(18), 13493.

6. Li, X. & Zhang, X. (2023). A comparative study of statistical and machine learning models on carbon dioxide emissions prediction of China. *Environmental Science and Pollution Research, 30*(55), 117485-117502.

7. Yildirim, M., Bingol, H., Cengil, E., Aslan, S. & Baykara, M. (2023). Automatic classification of particles in the urine sediment test with the developed artificial intelligence-based hybrid model. *Diagnostics, 13*(7), 1299.

8. Al Nuaimi, H.S., Acquaye, A. & Mayyas, A. (2025). Machine learning applications for carbon emission estimation. *Resources, Conservation & Recycling Advances, 27*, 200263.

9. Ma, Y., He, P.J., Lü, F., Zhang, H., Yan, S., Cao, D., Mao, H. & Jiang, D. (2024). Machine learning-based prediction of the CO_2 concentration in the flue gas and carbon emissions from a waste incineration plant. *ACS ES&T Engineering, 4*(3), 737-747.

10. Begum, A.M. & Mobin, M.A. (2025). A machine learning approach to carbon emissions prediction of the top eleven emitters by 2030 and their prospects for meeting Paris agreement targets. *Scientific Reports, 15*(1), 1-40.

11. Alhussan, A.A., Metwally, M. & Towfek, S.K. (2025). Predicting CO_2 emissions with advanced deep learning models and a hybrid greylag goose optimization algorithm. *Mathematics, 13*(9), 1481.

12. Ayaz, İ. (2024). Forecasting co_2 emissions with machine learning methods: Türkiye example and future trends. *NATURENGS MTU Journal of Engineering and Natural Sciences Malatya Turgut Ozal University, 5*(2), 82-87.

13. Uluocak, İ. (2025). Comparative study of emission prediction using deep learning models. *Çukurova Üniversitesi Mühendislik Fakültesi Dergisi, 40*(2), 337-346.

14. Aslan, E. (2024). Araçlarda CO_2 emisyonlarının farklı yapay sinir ağı modelleri kullanılarak tahminlerinin karşılaştırılması. *Çukurova Üniversitesi Mühendislik Fakültesi Dergisi, 39*(2), 309-324.

15. What Is ARIMA Modeling, (2023). *Master's in Data Science,* edX.org, [Online]. Available: https://www.mastersindatascience.org/learning/statistics-data-science/what-is-arima-modeling. Access date: 20.10.2025.

16. Koçak, H. (2024). Time series prediction of temperature using Seasonal Arima and LSTM models. *Gazi Journal of Engineering Sciences*, *9*(3), 574-584.

17. Kaur, J., Parmar, K.S. & Singh, S. (2023). Autoregressive models in environmental forecasting time series: A theoretical and application review. *Environmental Science and Pollution Research, 30*(8), 19617-19641.

18. Box, G.E.P., Jenkins, G.M. & Reinsel, G.C. (1994). *Time series analysis: forecasting and control.* 3rd edn. Prentice-Hall, Englewood Cliffs, NJ.

19. Hornik, K., Stinchcombe, M. & White, H. (1989). Multilayer feedforward networks are universal approximators. *Neural Networks*, *2*(5), 359-366.

20. Engelbrecht, A.P. (2007). *Computational intelligence: an introduction.* Wiley, New York.

21. Abdulkarim, S.A. & Engelbrecht, A.P. (2020). Time series forecasting with feedforward neural networks trained using particle swarm optimizers for dynamic environments. *Neural Computing and Applications, 33*(7), 2667-2683.

22. Milano, P. & Elettrotecnica, D. (2004). PSO as an effective learning algorithm for neural network applications. *Proceedings. ICCEA 2004. 3rd International Conference on Computational Electromagnetics and Its Applications,* , 557-560.

23. Tumse, S., Bilgili, M. & Sahin, B. (2022). Estimation of aerodynamic coefficients of a non-slender delta wing under ground effect using artificial intelligence techniques. *Neural Computing and Applications, 34*(13), 10823-10844.

24. Arora, I., Gambhir, J. & Kaur, T. (2020). Data normalisation-based solar irradiance forecasting using artificial neural networks. *Arabian Journal for Science and Engineering, 46*(2), 1333-1343.

25. Hochreiter, S. & Schmidhuber, J. (1997). Long short-term memory. *Neural Computation, 9*(8), 1735-1780.

26. Mathworks, (2020). *Long short-term memory networks.* https://www.mathworks.com/help/deeplearning/ug/longshort-term-memory-networks.html. Access date: 20.10.2025.

27. Mateus, B.C., Mendes, M., Farinha, J.T., Assis, R. & Cardoso, A.M. (2021a). Comparing LSTM and GRU models to predict the condition of a pulp paper press. *Energies, 14*(21), 6958.

28. Lynn, H.M., Pan, S.B. & Kim, P. (2019). A deep bidirectional GRU network model for biometric electrocardiogram classification based on recurrent neural networks. *IEEE Access, 7*, 145395-145405.